



NRC Publications Archive Archives des publications du CNRC

Electrocatalytic activity and durability of Pt/NbO₂ and Pt/Ti₄O₇ nanofibers for PEM fuel cell oxygen reduction reaction Senevirathne, Keerthi; Hui, Rob; Campbell, Stephen; Ye, Siyu; Zhang, Jiujun

This publication could be one of several versions: author's original, accepted manuscript or the publisher's version. / La version de cette publication peut être l'une des suivantes : la version prépublication de l'auteur, la version acceptée du manuscrit ou la version de l'éditeur.

For the publisher's version, please access the DOI link below. / Pour consulter la version de l'éditeur, utilisez le lien DOI ci-dessous.

Publisher's version / Version de l'éditeur:

<https://doi.org/10.1016/j.electacta.2011.11.005>

Electrochimica Acta, 59, pp. 538-547, 2011-11-09

NRC Publications Record / Notice d'Archives des publications de CNRC:

<https://nrc-publications.canada.ca/eng/view/object/?id=3cc6c10a-0963-490d-9475-d66141cfcb29>

<https://publications-cnrc.canada.ca/fra/voir/objet/?id=3cc6c10a-0963-490d-9475-d66141cfcb29>

Access and use of this website and the material on it are subject to the Terms and Conditions set forth at

<https://nrc-publications.canada.ca/eng/copyright>

READ THESE TERMS AND CONDITIONS CAREFULLY BEFORE USING THIS WEBSITE.

L'accès à ce site Web et l'utilisation de son contenu sont assujettis aux conditions présentées dans le site

<https://publications-cnrc.canada.ca/fra/droits>

LISEZ CES CONDITIONS ATTENTIVEMENT AVANT D'UTILISER CE SITE WEB.

Questions? Contact the NRC Publications Archive team at

PublicationsArchive-ArchivesPublications@nrc-cnrc.gc.ca. If you wish to email the authors directly, please see the first page of the publication for their contact information.

Vous avez des questions? Nous pouvons vous aider. Pour communiquer directement avec un auteur, consultez la première page de la revue dans laquelle son article a été publié afin de trouver ses coordonnées. Si vous n'arrivez pas à les repérer, communiquez avec nous à PublicationsArchive-ArchivesPublications@nrc-cnrc.gc.ca.





Electrocatalytic activity and durability of Pt/NbO₂ and Pt/Ti₄O₇ nanofibers for PEM fuel cell oxygen reduction reaction

Keerthi Senevirathne^{a,*}, Rob Hui^a, Stephen Campbell^b, Siyu Ye^c, JiuJun Zhang^{a,**}

^a Institute for Fuel Cell Innovation, National Research Council of Canada, 4250 Wesbrook Mall, Vancouver, B.C. V6T 1W5, Canada

^b Automotive Fuel Cell Cooperation Corp., 9000 Glenlyon Parkway, Burnaby, B.C. V5J 5J8, Canada

^c Ballard Power Systems, Inc., 9000 Glenlyon Parkway, Burnaby, B.C. V5J 5J8, Canada

ARTICLE INFO

Article history:

Received 19 September 2011

Received in revised form 1 November 2011

Accepted 2 November 2011

Available online 9 November 2011

Keywords:

Pt catalysts

Niobium oxide (NbO₂)

Titanium dioxide (Ti₄O₇) supports

Oxygen reduction reaction

PEM fuel cells

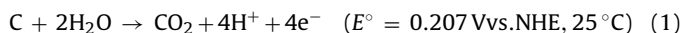
ABSTRACT

In this paper, we report the synthesis of both NbO₂ and Ti₄O₇ nanofibers using an electrospinning technique in an effort to use metal oxides as a possible replacement for carbon as PEM fuel cell catalyst supports. The synthesized nanofibers are physically characterized using several methods including XRD, SEM, TEM, BET, ICP-MS as well as XPS. The thermal, chemical, and electrochemical stabilities as well as the electronic conductivities of these two supports are also evaluated in order to check their feasibility as catalyst supports in the temperature range of 95–200 °C. Two catalysts, 20-wt% Pt/NbO₂ and 20-wt% Pt/Ti₄O₇, are prepared and tested for both ORR mass activity and stability in acidic solution. XPS measurements of samples analyzed before and after the durability tests suggest the formation of electronically insulating surface oxides, which can be partially responsible for both low ORR mass activity and catalyst durability.

Crown Copyright © 2011 Published by Elsevier Ltd. All rights reserved.

1. Introduction

In polymer electrolyte membrane (PEM) fuel cells, the most practical catalysts, which are used to catalyze the slow oxygen reduction reaction (ORR) at the cathode and the fuel (hydrogen) oxidation reaction (HOR) at the anode, respectively, are carbon supported Pt-based catalysts. Generally, use of carbon material as a catalyst support is due to its inherent large accessible surface area, well-developed mesoporous structure, as well as high electrical conductivity, which are of critical importance for both heterogeneous and homogeneous catalysis. Unfortunately, the major issue for carbon supported Pt catalysts is the electrochemical oxidation of carbon support [1] under fuel cell operation conditions according to Eq. (1) [2]:



The harsh conditions at the cathode include oxidative oxygen, hot water, acidic environment as well as high electrode potentials. These conditions are favorable to the oxidation of carbon support, especially in the temperature range of 95–200 °C. This type of electrochemical corrosion of carbon support will eventually result in

platinum (Pt) catalyst particle agglomeration and sintering in acidic media, leading to catalytic performance degradation. Moreover, carbon corrosion can also lead to electrically isolated Pt catalyst particles detached from carbon supports that provide no contribution to catalytic activity. The overall consequence is the reduced lifetime and poor performance of a PEM fuel cell.

In order to overcome this carbon corrosion challenge, developing alternative catalyst supports to replace carbon in polymer PEM fuel cells has received much attention in recent years. In the effort to develop non-carbon materials, high conductivity, strong support-catalyst nanoparticle interaction, and high surface area are key requirements for support materials to be used in Pt based electrocatalysts. In addition, properties such as chemical, thermal, and electrochemical stability also have to be taken into consideration when choosing a catalyst support material. For example, some metal oxides such as TiO₂ have received much attention owing to their chemical stability in acidic medium, thermal stability, and low cost. However, their electronic conductivities appear insufficient.

Recent studies have explored conductive NbO₂ and magneli phase titanium oxide (suboxides) materials such as Ti_nO_{2n-1} (4 < n < 10) as potential fuel cell catalyst supports. The magneli phases are known as Ebonex materials and are commercially available to purchase. Sasaki et al. [3] studied the use of carbon/niobium oxide composite (NbO₂ and/or Nb₂O₅) to form supported Pt monolayer catalyst (such as Pt/NbO₂-C), demonstrating that this Pt/NbO₂-C electrocatalyst was three times more active than that of commercially available Pt/C electrocatalyst, as well as having a

* Corresponding author. Tel.: +1 604 221 3000; fax: +1 604 221 3001.

** Corresponding author. Tel.: +1 604 221 3087; fax: +1 604 221 3001.

E-mail addresses: Senevirathne.k@gmail.com, keerthi.s@yahoo.com (K. Senevirathne), JiuJun.Zhang@nrc-cnrc.gc.ca (J. Zhang).

higher durability under oxidizing conditions up to 30,000 cycles in 0.1 M HClO₄. In another study, NbO₂/C was used to support Pt to form Pt/NbO₂/C catalyst for methanol oxidation. Its activity was compared with both Pt_{ML}Ru/C and commercially available Pt–Ru/C catalysts, and found that the mass activity of this catalyst, normalized by the total noble metal mass, was higher than both of these Pt–Ru/C catalysts. The result suggested that NbO₂ has a potential to be used as a support for Pt catalysts [4]. However, NbO₂ is still not thoroughly explored as a fuel cell catalyst support as is evident by the availability of only a few literature reports. Similarly, sub-stoichiometric titanium–oxygen compositions (magneli phases) have received considerable attention. Among these distinct oxides, Ti₄O₇ has been proposed and investigated as a possible Pt support material for PEM fuel cell cathodes owing to its high electrical conductivity, resistance to oxidation [5] and corrosion [6]. For example, Ebonex (Atraverda Ltd., UK), in which the main component is Ti₄O₇, has been widely studied as a conductive matrix in microelectrode arrays and as a substrate for electrode materials [7], and in ceramic electrodes [8]. Chen et al. [9] studied both Ebonex and pure Ti₄O₇ as viable replacements to carbon, and as supports for Pt, Ru, and Ir containing bifunctional catalysts for unitized regenerative fuel cells. It was discovered that both Ebonex and Ti₄O₇ showed limited electrochemical durability in 0.5 M H₂SO₄ followed by gradual loss of activity due to an increase in electronic resistance with time. Ioroi et al. [5] explored electrochemical performance of Pt/Ti₄O₇ catalyst under actual fuel cell operating conditions, and showed that Pt/Ti₄O₇ was equally as active as Pt/XC-72. They claim that given the initial electrochemical activity, Pt/Ti₄O₇ might be used as a corrosion-resistant anode and cathode catalyst in PEM fuel cells.

In this paper, we developed an electrospinning synthesis method to prepare both NbO₂ and Ti₄O₇ nanofibers and explored them as alternative Pt catalyst supports. Their chemical and thermal stabilities at 95 °C and 200 °C, as well as electrochemical stability at 30 °C were investigated. To validate their catalytic activity and durability toward oxygen reduction reaction (ORR), these catalysts were individually coated on an electrode to form catalyst layers for ORR testing using conventional rotating disk electrode technique.

2. Experimental methods

Nanofibers of niobium oxide (NbO₂) and titanium dioxide (Ti₄O₇) were synthesized using a similar route employed in the synthesis of TiO₂ [10] and several other oxides such as Al₂O₃ [11], V₂O₅, ZnO [12], and doped-oxides [13,14]. The synthesis involved electrospinning of a mixture of metal alkoxides, niobium(V) ethoxide or titanium(IV) isopropoxide, and polymer polyvinyl pyrrolidone (PVP) in anhydrous ethanol. The PVP polymer served to add a viscoelastic behavior to the precursor solution. This helped to maintain a continuous spinning jet of polymer/metal alkoxide composite.

In a typical synthesis of niobium oxide nanofibers, 1.5 mL of niobium(IV) ethoxide (Nb(oet)₅, Alfa Aesar, 99.9%) was mixed with 3.0 mL of anhydrous ethanol (Commercial Alcohols Inc.) and 3.0 mL of glacial acetic acid (Fisher Scientific) with magnetic stirring for 15 min to form a precursor solution. In a separate vial, 0.3 g of polyvinyl pyrrolidone (PVP, Across Organics, M.W. 130,000) was dissolved in 7.5 mL of anhydrous ethanol and sonicated for 15 min to remove trapped air. This polymer solution was then gradually mixed with the precursor solution with stirring in a tightly capped glass vial to form the electrospinning solution. For the electrospinning process, this electrospinning solution was loaded into a 20.0 mL dry glass syringe equipped with a 0.04 mm gauge blunt ended stainless steel needle. The spinning process was carried out at a solution-feeding rate of 0.7 mL per hour with the application

of 12 kV at the needle tip. A piece of Ni foil placed at a distance of 6.0 cm from the needle tip was used as a sample collector. The collected fibers were left overnight in air in order to allow complete hydrolysis of metal ethoxide precursors. After that, the samples were calcined in air at 550 °C for 3 h in a digitally controlled furnace in order to achieve a complete decomposition, and removal of the PVP polymer, and crystallization of niobium oxide. The pre-calcined fibers were then reduced at 900 °C for 30 min in a flow of H₂:N₂ (1:1) to yield NbO₂ fibers. A similar fabrication procedure was followed in order to synthesize TiO₂ nanofibers using titanium(IV) isopropoxide (Ti(OiPr)₄, 98%, Acros) as the precursor. For Ti₄O₇ fiber synthesis, the obtained as-spun TiO₂ fibers were first calcined at 550 °C for 3 h in air, and then reduced at 1050 °C for 6 h in a continuous stream of H₂:N₂ (1:1) to form Ti₄O₇ fibers.

For synthesizing metal oxide supported Pt catalysts, Pt deposition on NbO₂ or Ti₄O₇ support was performed using the NaBH₄ reduction method. Briefly, a known amount of oxide support was first dispersed in absolute ethanol by sonicating for 1 h in a sonicator bath. Then, the required amount of chloroplatinic acid hexahydrate (H₂PtCl₆, Sigma–Aldrich) was mixed with the oxide support dispersion (with a target of 20-weight percent (20-wt%) Pt loading) and stirred for 2 h to form Pt precursor-support dispersion solution. Excess of 0.1 M NaBH₄ solution, prepared by dissolving the required amount of NaBH₄ in absolute ethanol, was added into this support dispersion solution and stirred 15 h to complete Pt deposition. The Pt catalyst fibers formed (Pt supported on the metal oxide support (NbO₂ or Ti₄O₇), abbreviated as 20-wt% Pt/NbO₂ or 20-wt% Pt/Ti₄O₇), were collected, purified by centrifugation at 10,000 rpm for 15 min, and then washed with de-ionized water three times. Finally, the 20-wt% Pt/NbO₂ or 20-wt% Pt/Ti₄O₇ fiber catalyst was dried in an oven at 60 °C until a dry powder was formed.

For physical characterization of the synthesized samples, a Bruker D8 Advance X-ray diffractometer equipped with a Cu K α anode source was used for X-ray powder diffraction (XRD) analysis. In this measurement, a thin smear of vacuum grease was applied on zero background quartz (0 0 0 1) holder on which a uniform layer of sample powder was placed. The X-ray patterns were identified by matching with available phases from the EVA diffraction database.

For transmission electron microscope (TEM) imaging, a Hitachi H7600 microscope, operated at 100 kV, was employed. For specimen preparation, the nanofiber powder was dispersed in ethanol by sonication in a sonicator bath for approximately 5 min and then a drop of the resultant dispersion was placed on a carbon-coated copper grid and allowed to dry at room temperature under ambient conditions. The images were collected under the bright field mode. For scanning electron microscope (SEM) imaging, a Hitachi 3500-S instrument was used. For SEM specimen preparation, a small amount of powder was spread on a carbon tape adhered to aluminum specimen holder. The Quartz PCI software was used to collect and record the images.

For thermogravimetric analysis (TGA), A Perkin-Elmer Pyris 1 thermogravimetric analyzer was used to determine the oxidation temperature of NbO₂ and Ti₄O₇ nanofibers. During the measurement, the nanofiber sample was heated up to 750 °C with a temperature ramp rate of 10 °C min⁻¹ in continues flow of air.

A Beckman Coulter SA 3100 Surface Area Analyzer was used in surface area and porosity analyses. Powder sample was out-gassed at 120 °C for 30 min prior to analysis. The specific surface areas and pore size distribution of the samples were evaluated using the Brunauer, Emmet, and Teller (BET) method and the Barrett, Joyner, and Halenda (BJH) method, respectively.

Room temperature electronic conductivity measurements of both NbO₂ and Ti₄O₇ nanofiber powders were conducted using a specially designed gold-coated copper cell connected to a Solatron Analytical 1252A frequency response analyzer coupled with

Solatron SI 1287 potentiostat electrochemical interface. A constant pressure (2.55 kg cm^{-2}) was applied on the sample during the measurements in order to achieve proper contacts among the nanofibers tested as well as between the gold-coated copper and the nanofiber sample. The Z-plot and Z-view software were used to collect the bulk resistance data. The resistance of porous powders were measured and then converted into the conductivity. The conductivities obtained here should not reflect the materials' crystal conductivity values because the sample disks had a porous structure. This porous structure may be more close to those in fuel cell catalyst layers. Therefore, the conductivities reported here are those at specific conditions such as a fixed pressure and temperature.

For investigating the degradation mechanism of catalyst supports, X-ray photoelectron spectroscopy (XPS) was used to measure the XPS spectra before and after the electrochemical durability testing. A gold mesh, on which the NbO_2 fiber powder was deposited, was used as the working electrode. XPS measurements were performed on a Leybold Max 200 spectrometer using a non-monochromatic Mg K α radiation operated at 200 W (10 kV, 20 mA). All data were calibrated with respect to C 1s excitation in order to account for charging effects by the electron beam. Narrow scans for Nb were acquired in 0.2 eV step sizes. The XPS spectra were fitted and evaluated with XPS PEAK 4.1 software and a mixed Gaussian-Lorentzian function was used to deconvolute the peak shape. The Shirley function was applied in order to subtract the background.

For the evaluation of chemical stability of the synthesized support samples, the samples were tested according to the protocol outlined as follows: The nanofiber material (0.2 g), mixed with 50 mL of 1 M H_2SO_4 in a round bottom flask fitted with refluxing set up, and refluxed while stirring magnetically at 95°C for 24 h in a silicone oil bath heated with a digitally controlled hot plate. After 24 h of refluxing, the solution and un-dissolved solid in the mixture were separated. Then, the collected solution was analyzed by elemental analysis (ICP/MS), and un-dissolved solid collected was analyzed using powder X-ray diffraction (PXRD) analysis. For 200°C solubility test, a specially designed solubility test apparatus was used. Briefly, the oxide support was mixed with 50 mL of 1 M H_2SO_4 in a zirconium autoclave fitted with a thermocouple. The tightly capped autoclave was pressurized with N_2 gas up to 200 psi and was immersed in a pre-heated silicon oil bath at 200°C . Inside temperature was monitored using a thermocouple attached to a temperature read-out. Refluxing was continued for 2 h at 200°C followed by recovery of solution for elemental analysis.

For electrochemical measurements, a conventional three-electrode test cell was used. This cell contained three electrodes, one was a catalyst-coated glassy carbon-working electrode (GCE, 0.5 cm diameter and 0.20 cm^2 geometric surface area, Pine Instruments), the second was a Pt wire as the counter electrode, and the third was a reversible hydrogen electrode (RHE) as the reference electrode. For working electrode preparation, a known amount of catalyst powder was dispersed in a mixture of isopropyl alcohol (IPA) and de-ionized water (95:5 ratio by volume), followed by sonication in a sonicator bath for 1 h. Then the required volume of the ink was placed on GC electrode and dried to form a catalyst layer with a loading of $47.8 \mu\text{gPt cm}^{-2}$. A Nafion[®] coat was then cast by pipetting out $7.0 \mu\text{L}$ of 1:100 dilution of 5 wt% Nafion[®] in methanol on to the top of catalyst layer covered electrode. The freshly prepared electrode was subjected to potential cycling for 20 cycles in N_2 -purged 0.1 M HClO_4 electrolyte in the range of 0.05–1.2 V vs. RHE at a scan rate of 20 mV s^{-1} . Electrochemical durability testing of catalyst was carried out at 20 mV s^{-1} with 1000 full cycles in the potential range of 0.05–1.2 V vs. RHE. The electrochemical surface area (ECSA) was

calculated based on the H_2 adsorption–desorption peaks observed between 0.05 and 0.4 V using a hydrogen adsorption–desorption charge of $210 \mu\text{C cm}^{-2}$ as the standard charge for a smooth Pt surface. Oxygen-reduction reaction (ORR) experiments were carried out in O_2 -saturated 0.1 M HClO_4 electrolyte at a scan rate of 5 mV s^{-1} and a 1600-rpm of electrode rotation rate in the potential range of 0.4–1.2 V vs. RHE. The current–voltage curve at anodic scan was used for ORR activity calculation. The ORR mass activity (mA/mgPt) was calculated using the current at 0.9 V vs. RHE and the Pt loading on the working electrode.

All electrochemical measurements were performed at 30°C using a Solartron multistat instrument, controlled with Corrware software (Scribner Associates Inc., USA).

3. Results and discussion

3.1. Structural and morphological characterization of NbO_2 and Ti_4O_7 nanofibers

Powder X-ray diffraction (PXRD) analysis was used to collect structural information of nanofibers of both NbO_2 and Ti_4O_7 , and the observed XRD powder patterns are shown in Fig. 1. As mentioned previously, NbO_2 was prepared by reducing Nb_2O_5 in H_2/N_2 , and the XRD pattern of the resultant powder after reduction, shown in Fig. 1(a), is marked as “initial”, which matches very well with calculated pattern of NbO_2 . It can be seen that besides the NbO_2 peaks, no other additional peaks can be observed, indicating that the synthesis here can give a pure phase NbO_2 . In addition, it can also be observed that the synthesized NbO_2 fibers are highly crystalline, as evidenced by the sharp diffraction peaks. This can be expected as these fibers were calcined at 550°C and then reduced at 900°C in the presence of H_2 . Similarly, TiO_2 nanofibers, obtained by calcination of electrospun fibers at 550°C , were transformed into Ti_4O_7 fibers upon reductive treatment at 1050°C followed by a structural identification using XRD (Fig. 1(b)).

Fig. 2 shows the BET N_2 adsorption–desorption isotherm plots ((a) and (b)) and percentage pore distribution as a function of pore diameter ((c) and (d)) of NbO_2 and Ti_4O_7 nanofibers, respectively. Similar plots of Nb_2O_5 and TiO_2 nanofibers have been also included in Fig. 2 for comparison. The surface areas of Nb_2O_5 and TiO_2 nanofibers decreased from 54 to $13 \text{ m}^2/\text{g}$ and 51 to $6 \text{ m}^2/\text{g}$, respectively, after they were transformed into NbO_2 and Ti_4O_7 nanofibers. However, the surface areas reported here for NbO_2 and magneli-phase Ti_4O_7 nanofibers are still much higher than that of commercially available NbO_2 ($\sim 1 \text{ m}^2/\text{g}$), and literature reported Ti_4O_7 ($\sim 2 \text{ m}^2/\text{g}$) [15]. The decrease in surface areas can be attributed to both surface smoothing as well as fiber growth induced by reductive heat treatment at higher temperatures (900 – 1050°C), as evidenced by TEM images (Fig. 3). The pore size distribution plots in Fig. 2 clearly indicate that a large fraction of available pores belong to meso-regime (2–50 nm) for both metal oxides. However, the pore distribution, after forming NbO_2 or Ti_4O_7 , at a given pore diameter, dramatically decreases as a result of disappearance of meso-pores, which were present in Nb_2O_5 or TiO_2 , possibly due to high temperature reductive treatments.

The morphology of metal oxide nanofibers was determined using both the scanning and transmission electron microscopic techniques (SEM and TEM). Fig. 3 shows the TEM images of both NbO_2 and Ti_4O_7 nanofibers together with SEM images of the as-spun respective metal oxide nanofibers. The TEM images of calcined NbO_2 and Ti_4O_7 nanofibers are shown as insets into Fig. 3(c) and (d), respectively. The nanofibrous nature of the as-spun (metal oxide/PVP composite) nanofibers, which could stretch

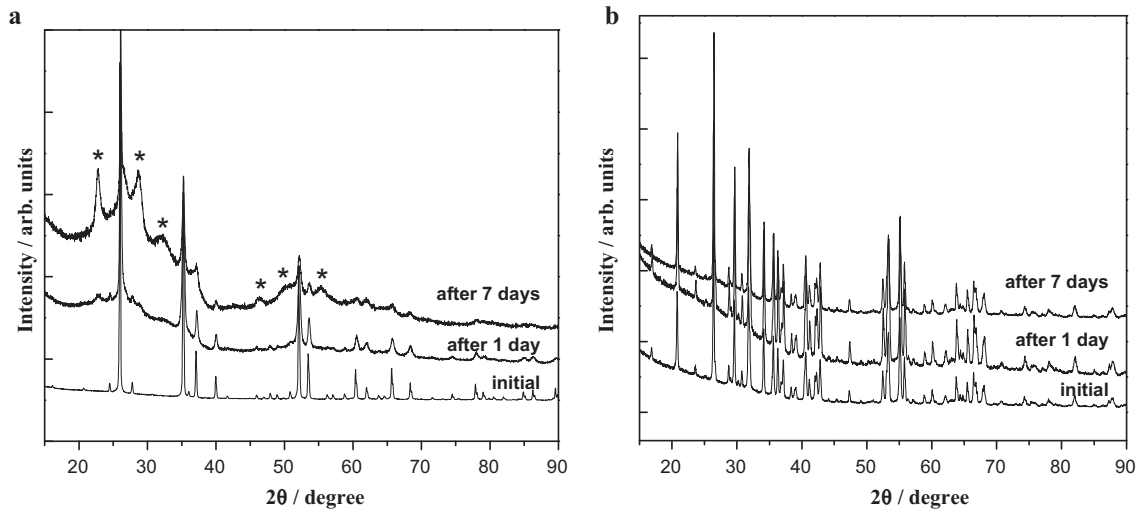


Fig. 1. Powder X-ray diffraction (PXRD) patterns of NbO_2 (a) and Ti_4O_7 (b) nanofibers (marked as “initial”) formed after reduction in H_2/N_2 . Nanofibers heat-treated at 200°C in air for 1 day and 7 days are also shown. Peaks marked with asterisks belong to Nb_2O_5 phase.

up to several microns or even centimeters with a narrow polydispersion, can be clearly seen (Fig. 3(a) and (b)). The difference of fiber thickness before and after calcination seems not significant. However, the fiber thickness of both metal oxides increases upon

the reduction treatment at high temperatures (900 and 1050°C for NbO_2 and Ti_4O_7 , respectively). For example, compared Fig. 3(c) to its inset, and Fig. 3(d) to its inset, the NbO_2 nanofiber diameter grows approximately from 50 nm to 150 nm after the reduction

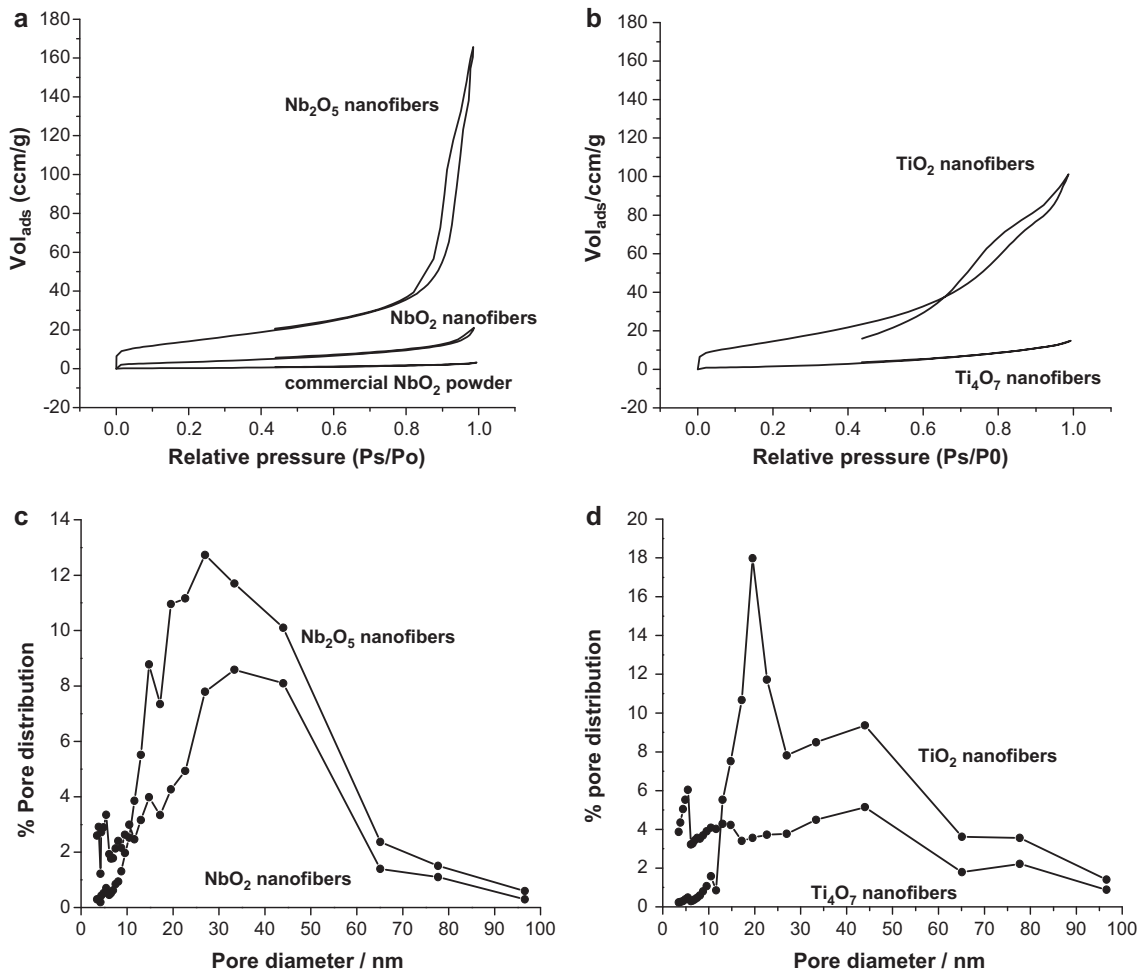


Fig. 2. Nitrogen adsorption–desorption isotherms of NbO_2 (a) and Ti_4O_7 (b) nanofibers along with isotherms for Nb_2O_5 and TiO_2 nanofibers shown for comparison. Plots (c) and (d) represent percentage pore distributions as a function of pore diameter.

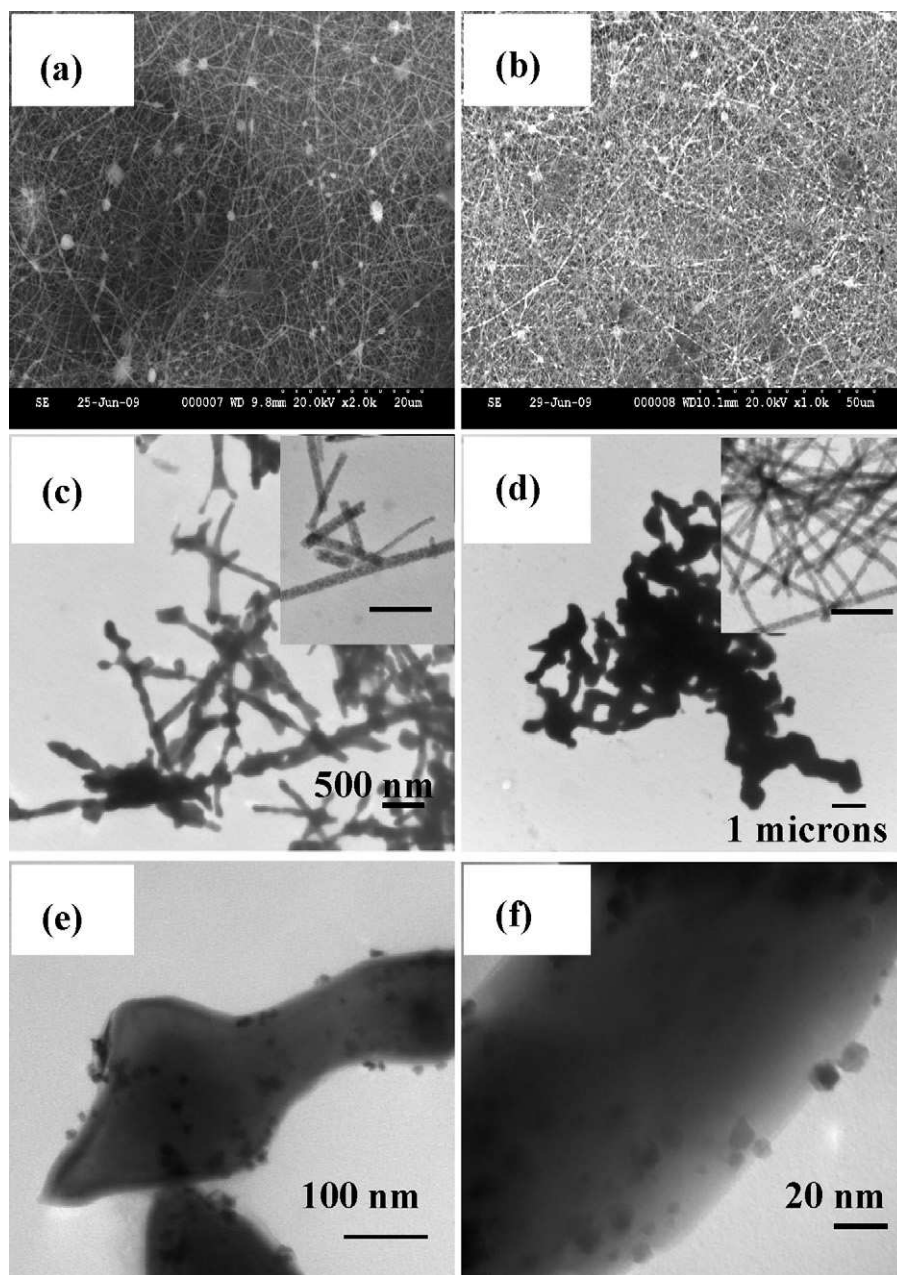


Fig. 3. Scanning and transmission electron microscopic images of NbO_2 and Ti_4O_7 nanofibers. (a) as-spun $\text{Nb}_2\text{O}_5/\text{PVP}$ composite, (b) as-spun TiO_2/PVP composite, (c) NbO_2 nanofibers, (d) Ti_4O_7 nanofibers, (e) 20-wt% Pt/NbO_2 , and (f) 20-wt% $\text{Pt}/\text{Ti}_4\text{O}_7$.

treatment, and the Ti_4O_7 fiber grows even up to micron size, and at the same time, the fibers become more like bulbous features. Mechanistic aspects of this growth have not been investigated here. However, high temperature sintering might be a reasonable explanation.

Fig. 3(e) and (f) shows the Pt catalyst particle distribution on the nanofibers. It seems that this Pt dispersion is not as uniform as expected. The average Pt particle size is 7.0 ± 1.2 nm. The inhomogeneity of the Pt particles may be rationalized by the lower surface roughness of nanofibers that is caused by the reduction treatment. Furthermore, the NaBH_4 reduction method for Pt deposition may also be responsible for poor dispersion and poly-dispersity of Pt particles. Relatively low surface area of nanofibers along with the absence of coordinating agents to prevent agglomeration in the reaction medium may caused the agglomeration of Pt particles.

3.2. Chemical stability in 1 M H_2SO_4

Chemical stability in terms of solubility and phase integrity of NbO_2 and Ti_4O_7 nanofibers were tested in 1 M H_2SO_4 at 95 and 200 °C, separately and metal concentration and percentage solubility have been summarized in the Table 1. The percentage solubility of NbO_2 and Ti_4O_7 in 1 M H_2SO_4 was significantly low (<1%) at both 95 and 200 °C under the applied experimental conditions. It was also found that this chemical dissolution process in acid did not cause significant changes in the bulk crystalline structure of NbO_2 and Ti_4O_7 as well. However, it is worthwhile to note the possibility of surface oxidation, which is difficult to evaluate by XRD measurements. These insignificant solubilities of both NbO_2 and Ti_4O_7 in acidic solution suggest that they are favorable enough for fuel cell applications in the range of 95–200 °C if they are to be used as catalyst supports.

Table 1ICP/MS elemental analysis data for NbO₂ and Ti₄O₇ nanofibers refluxed at 95 and 200 in 1 M H₂SO₄ for 24 and 2 h, respectively.

Metal oxides	Metal concentration in solution (mg mL ⁻¹)		Percentage solubility (wt%)	
	95 °C ^a	200 °C ^b	95 °C	200 °C
NbO ₂	0.004	0.016	0.12	0.51
Ti ₄ O ₇	0.006	0.028	0.25	0.70

Superscripts 'a' and 'b' denote refluxing in 1 M H₂SO₄ for 24 and 2 h, respectively

3.3. Thermal stability of NbO₂ and Ti₄O₇ nanofibers as a function of temperature in air

Thermal stability of NbO₂ and Ti₄O₇ nanofibers was determined by employing thermogravimetric analysis (TGA) in air at a temperature range of 30–750 °C and the data plots are shown in Fig. 4. The apparent weight gains observed for both NbO₂ and Ti₄O₇ were probably induced by their oxidation into most stable Nb₂O₅ and TiO₂. The gain of NbO₂ was about 6%, which is slightly less than the theoretical value (6.4%). This difference in weight gain might be due to the presence of remnant Nb₂O₅, which may have been formed by surface oxidation in the initial NbO₂. Similarly, Ti₄O₇ showed a 6.2% weight gain, which is 0.9% higher than that of the theoretical value (5.3%). It is still not fully understood yet about this difference. For NbO₂ phase transformation, TGA data show the largest weight gain at 300 °C as determined from derivative curves of TGA data. However, the transformation initiates around 150 °C, which is well below 200 °C and reaches a completion at 300 °C. This result indicates that NbO₂ may only be used as a support for PEM fuel cell catalysts with a operational temperature less than 150 °C. Interestingly, Ti₄O₇ phase transformation maximum is relatively higher than that of NbO₂ nanofibers and locates around 550 °C, and this material does not show any potential thermal oxidation below 300 °C, which is in agreement with the literature reported data [9]. This indicated that the thermal stability of Ti₄O₇ is acceptable to use it as PEM fuel cell support in the fuel cell desired temperature range of 95–200 °C.

To further evaluate the phase transformation of both NbO₂ and Ti₄O₇ fibers, we conducted prolonged heat treatment analysis for NbO₂ and Ti₄O₇ nanofibers in air at 200 °C from 1 to 7 days. It was observed from PXRD data shown in Fig. 1 that 1-day heat treatment could induce a slight phase transformation of NbO₂ nanofibers, which is indicative by the appearance of new diffraction peaks.

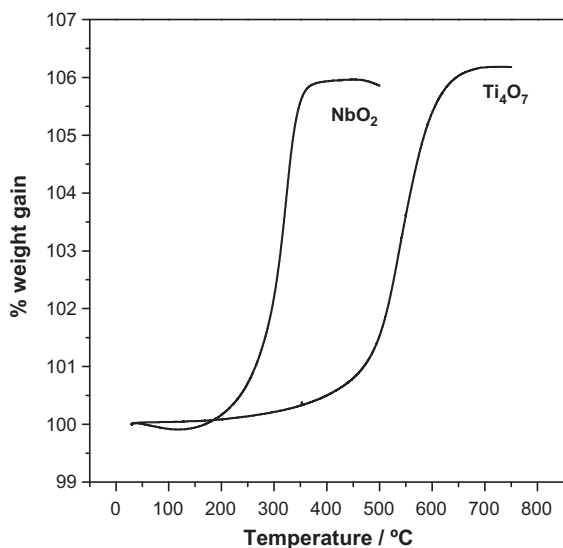


Fig. 4. Thermogravimetric analysis data of NbO₂ and Ti₄O₇ nanofibers heated in air up to 500 °C and 750 °C, respectively.

Newly appeared peak pattern matches very well with the peak position and intensity of calculated pattern of Nb₂O₅. Subsequent peak broadening was observed as a result of new phase formation. The breath of peaks is indicative of nanocrystalline domains that form new nanofiber structure (Fig. 1(a)). Further heating at the same temperature for longer period of time (for example, 7 days) could increase the peak intensities of Nb₂O₅ phase while decrease that of NbO₂ phase. However, commercially available NbO₂ that was subjected to the similar heat treatments (surface area ~ 1 m²/g, Aldrich) showed no visible phase transformation according to PXRD analysis (data not shown). It is still not clear why NbO₂ nanofibers thermally behave differently from NbO₂ powders. We speculate that either the relatively high surface area (13 vs. 1 m²/g) possesses a higher surface energy, leading to an increase in the transformation rate of NbO₂ nanofibers, or the synthesis method plays a vital role in the stability of NbO₂.

Nevertheless, Ti₄O₇ nanofibers showed a different behavior relative to NbO₂ fibers under the similar heat treatment conditions. No phase transformation could be observed even after heating at 200 °C for 7 days in air, which was evidenced by unchanged PXRD patterns (Fig. 1(b)). It is possible that the phase transformation actually occurs on the surface, which is undetectable by PXRD. However, as a bulk, the phase still retained as Ti₄O₇. These observations are in good agreement with the TGA results obtained for both NbO₂ and Ti₄O₇ nanofibers.

3.4. Electrical conductivity of NbO₂ and Ti₄O₇ nanofiber supports

The bulk electrical conductivities of both NbO₂ and Ti₄O₇ nanofibers were measured in order to evaluate the feasibility of using these materials as PEM fuel cell supports. The room temperature conductivities of NbO₂ and Ti₄O₇ nanofibers are 6.9 × 10⁻⁶ and 3.4 × 10⁻⁵ S cm⁻¹, respectively. For comparison, bulk conductivity of commercially available Ebonex was also measured using the same set-up, and the resultant conductivity was 3.2 × 10⁻⁵ S cm⁻¹, which is similar to that of the observed conductivity of Ti₄O₇ nanofibers. However, the observed conductivities of both NbO₂ and Ti₄O₇ nanofibers are significantly lower than those reported in the literature, mainly because the literature reported values were derived from single crystal materials. Moreover, Gallego and Thomas [16] showed that NbO₂ films prepared by sputtering, which was consisted of NbO₂ and some Nb₂O₅, had conductivity values ranging from 10⁻³ to 10⁻⁹ S cm⁻¹.

3.5. Electrochemical performance and stability of NbO₂ and Ti₄O₇ nanofiber supports

Fig. 5 shows the cyclic voltammograms (CVs) acquired for a thin layer of NbO₂ (a) and Ti₄O₇ (b) nanofiber supports fabricated on a glassy carbon electrode in N₂-saturated 0.1 M HClO₄ solution. The potential was scanned between 0.05 and 1.2 V vs. RHE at a scan rate of 20 mV s⁻¹ in N₂ atmosphere. Obviously, no pronounced oxidation–reduction current peaks were observed. The reasons for observed slight difference in the shapes of CVs of NbO₂ nanofiber support before and after durability are not fully known. The absence of oxidation peaks in both NbO₂ and Ti₄O₇ demonstrated that they are reasonably stable in acidic medium in the applied potential

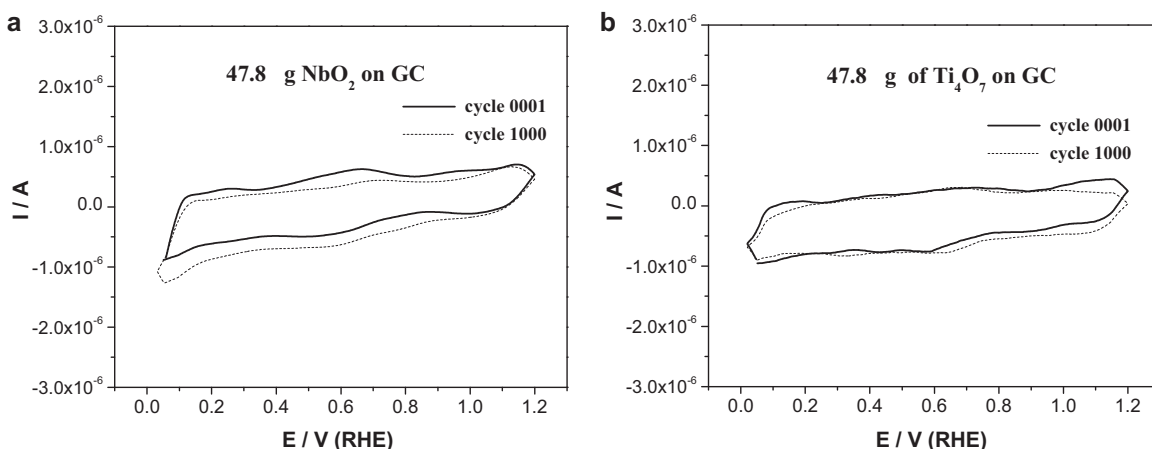


Fig. 5. Cyclic voltammograms of NbO₂ (a) and Ti₄O₇ (b) nanofibers on a glassy carbon electrode (area: 0.20 cm²) in N₂-saturated 0.1 M HClO₄ at 30 °C with a potential scan rate of 20 mV s⁻¹. Metal oxide loading: 47.8 μg cm⁻² for both NbO₂ and Ti₄O₇ nanofibers.

range and make them distinct from metal carbides i.e. TiC [17] or WC [18] reported in the literature.

3.6. Electrochemical performance and stability of Pt/NbO₂ and Pt/Ti₄O₇ nanofiber catalysts

Fig. 6(a) and (b) shows the CVs of Pt/NbO₂ and Pt/Ti₄O₇, respectively, recorded at 30 °C during continuous potential cycling between 0.05 and 1.2 V in N₂-saturated 0.1 M HClO₄ solution. The CV curves for both catalysts exhibit typical cyclic voltammograms with clear hydrogen adsorption–desorption and oxidation–reduction regions. However, those regions are prominent and well-defined in CV curves of Pt/Ti₄O₇ catalyst as the electrical conductivity of Ti₄O₇ is known to be higher than that of NbO₂ ($3.4 \times 10^{-5} \text{ S cm}^{-1}$ vs. $6.9 \times 10^{-6} \text{ S cm}^{-1}$). Therefore, the current generated by Pt catalysts is better conducted through the Pt/Ti₄O₇ catalyst layer into the GC electrode.

In order to test catalyst stability, cyclic voltammetric scanning between 0 and 1.2 V vs. RHE was carried out. Then the electrochemical surface areas (ECSAs) were calculated from the hydrogen adsorption–desorption region, as a function of CV cycle number (Fig. 7). It can be seen that both Pt/NbO₂ and Pt/Ti₄O₇ catalysts undergo a reduction in ECSA with increasing number of potential

cycles, suggesting degradation in the electrochemical environment. However, percentage ECSA loss of Pt/NbO₂ catalyst is even larger than that of Pt/Ti₄O₇ after 1000 potential cycles (62 vs. 23%). This ECSA drop may be attributed to two major factors: (1) the surface of support becomes quite resistant due to the formation of less conductive oxide layers (Nb₂O₅ and TiO₂, respectively), and (2) Pt particle dissolution and subsequent agglomeration to yield larger particles [19].

3.7. ORR activity of Pt/NbO₂ and Pt/Ti₄O₇ nanofiber catalysts

For ORR activity and stability, both Pt/NbO₂ and Pt/Ti₄O₇ nanofiber catalysts were tested using a rotating disk electrode technique in an O₂-saturated 0.1 M HClO₄ solution at 30 °C. The obtained current–voltage curves at different electrode rotation rates are shown in Fig. 8. Fig. 8(a) shows the ORR curves before the potential cycling of Pt/NbO₂ catalyst in a N₂-saturated 0.1 M HClO₄ solution, and (b) shows that ORR curves after the 1000 CV cycling in the potential range of 0–1.2 V vs. RHE. Similarly, Fig. 8(c) and (d) shows the ORR curves for Pt/Ti₄O₇ catalyst. As expected from diffusion theory, the increase in diffusion current with increasing electrode rotation rate can be observed. It can be clearly seen that after the 1000 CVs, the ORR cur-

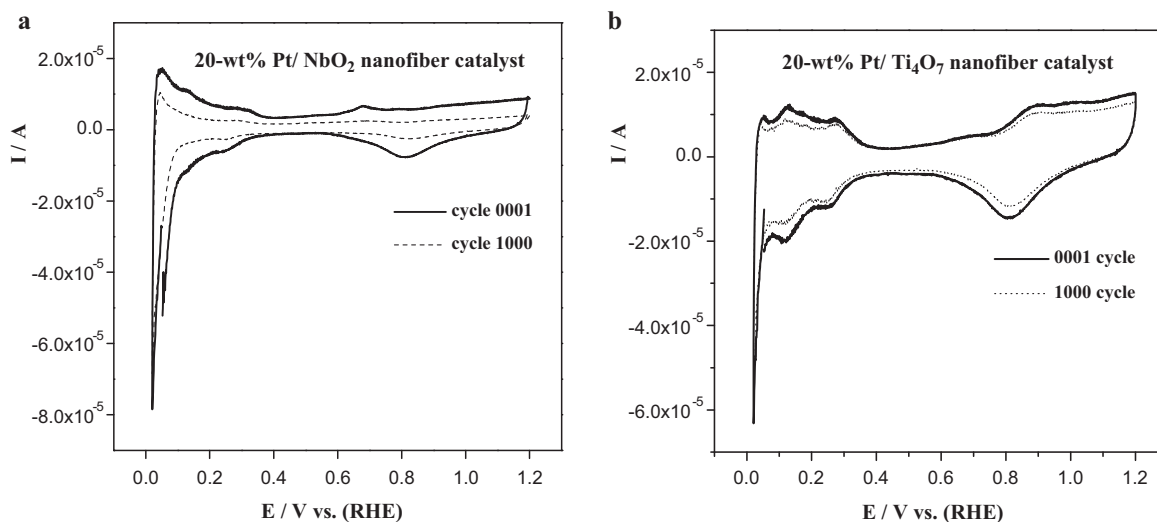


Fig. 6. Cyclic voltammograms of 20-wt% Pt/NbO₂ (a) and 20-wt% Pt/Ti₄O₇ (b) catalysts before and after durability testing, on a glassy carbon electrode (area: 0.20 cm²) recorded in N₂-saturated 0.1 M HClO₄ at 30 °C with a scan rate of 20 mV s⁻¹. Pt loadings: 47.8 μg Pt cm⁻² for both Pt/NbO₂ and Pt/Ti₄O₇.

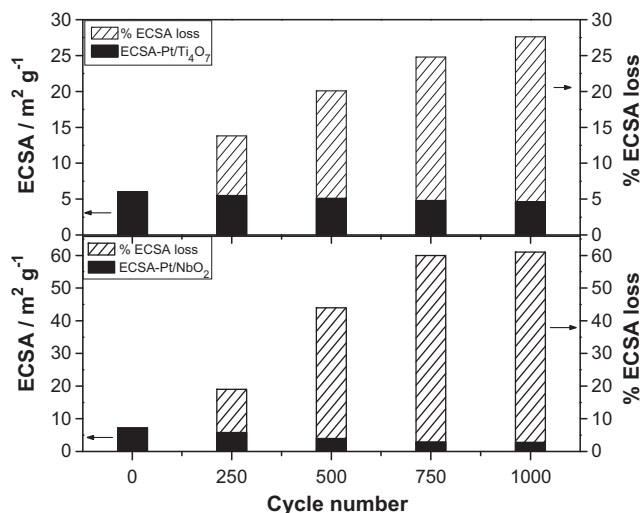


Fig. 7. Plots of the electrochemical Pt surface area (ECSA) and the percentage ECSA loss as a function of number of potential cycles.

rent is reduced significantly, indicating the catalyst activity has decreased.

For a more quantitative estimation, the ORR mass activities were calculated using the currents measured at 0.9 V vs. RHE of the anodic sweep at 1600 rpm. The onset potential occurred around 0.97 V for Pt/NbO₂ catalyst before durability test and remained

almost the same after durability test. The mass activity of Pt/NbO₂ catalyst dropped significantly, from 3.0 to 1.3 mA/mg Pt after durability testing, and corresponded to a loss of 57% of ORR mass activity. Similarly, ORR activity of Pt/Ti₄O₇ catalysts also drastically drops from 11.1 to 1.6 mA/mg Pt after the durability test, which corresponds to 86% loss of ORR mass activity.

3.8. Mechanism understanding using XPS measurements

To understand the possible cause of low mass activity and severe degradation of Pt/NbO₂ catalyst, the surface structural properties of NbO₂ nanofibers were examined before and after the durability test, conducted under potential cycling in N₂-saturated 0.1 M HClO₄ in the potential range of 0.4–1.2 V for 2000 cycles, using the X-ray photoelectron spectroscopy (XPS) technique. The surface chemical composition and any changes to oxidation state of Nb (either Nb⁴⁺ or Nb⁵⁺) would give some clues for understanding the low mass activity of Pt/NbO₂ catalyst and its degradation mechanism. Fig. 9 shows the valence band XPS spectra of NbO₂ nanofibers recorded before and after the durability test. The XPS spectrum acquired before potential cycling shows a peak at binding energy 207.8 eV that corresponds to Nb⁵⁺ spin-orbit doublet. A less prominent shoulder that appears at 206 eV corresponds to Nb⁴⁺ [15]. We believe that this Nb⁵⁺ should have come from surface Nb₂O₅, which is an electronic insulating Nb₂O₅ material. This observation indicates that part of the NbO₂ nanofiber surface has been oxidized into Nb₂O₅ even before subjecting to electrochemical potential cycling. This may be considered the factor limiting the

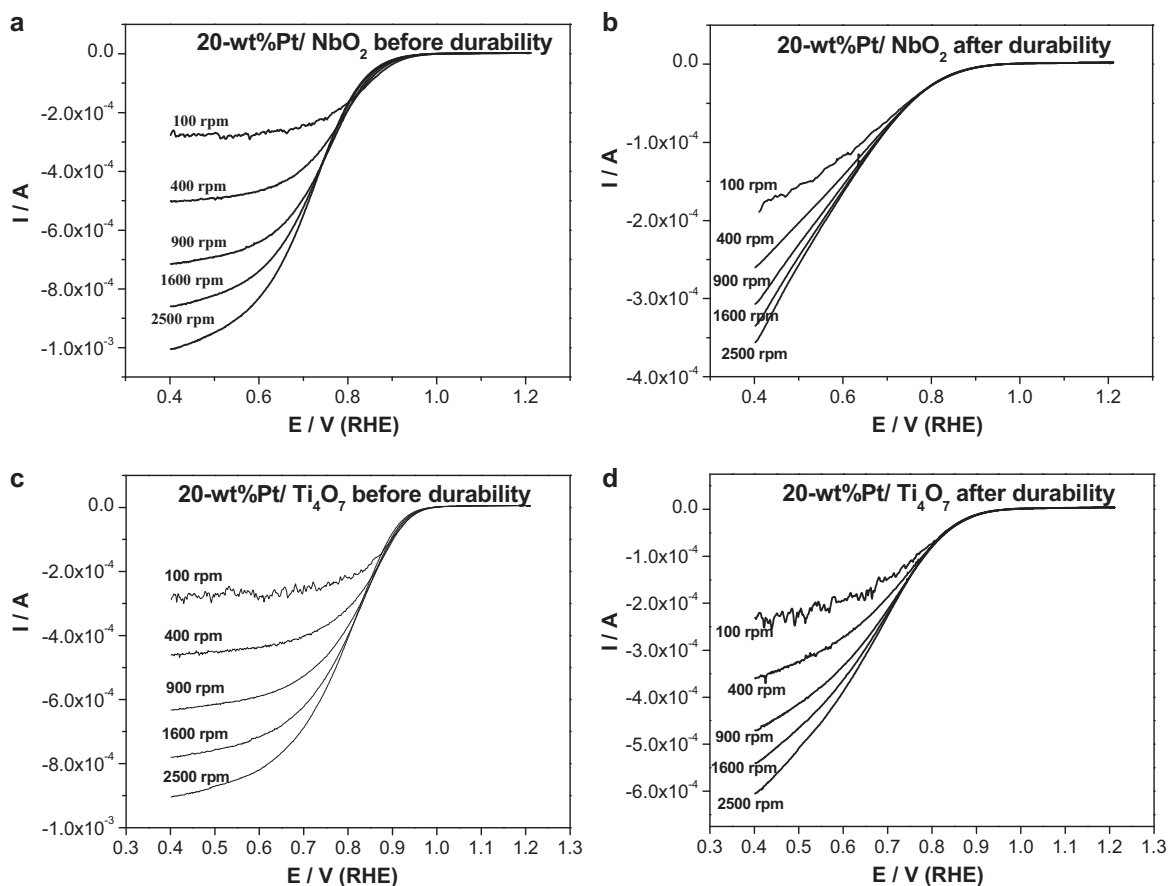


Fig. 8. ORR curves on 20-wt% Pt/NbO₂ and 20-wt% Pt/Ti₄O₇ nanofiber catalysts. (a) Pt/NbO₂, before durability test of cyclic voltammetric cycling for 2000 cycles in N₂-saturated 0.1 M HClO₄ solution at 20 mV s⁻¹, (b) Pt/NbO₂, after durability test, (c) Pt/Ti₄O₇, before durability test, (d) Pt/Ti₄O₇, after durability test. Recorded on a glassy carbon electrode (0.20 cm²) coated with the catalyst at different electrode rotation rates in O₂-saturated 0.1 M HClO₄ for 1000 cycles. Scan rate: 5 mV s⁻¹. Catalyst loadings for both 20-wt% Pt/NbO₂ and 20-wt% Pt/Ti₄O₇ are 47.8 μg Pt cm⁻².

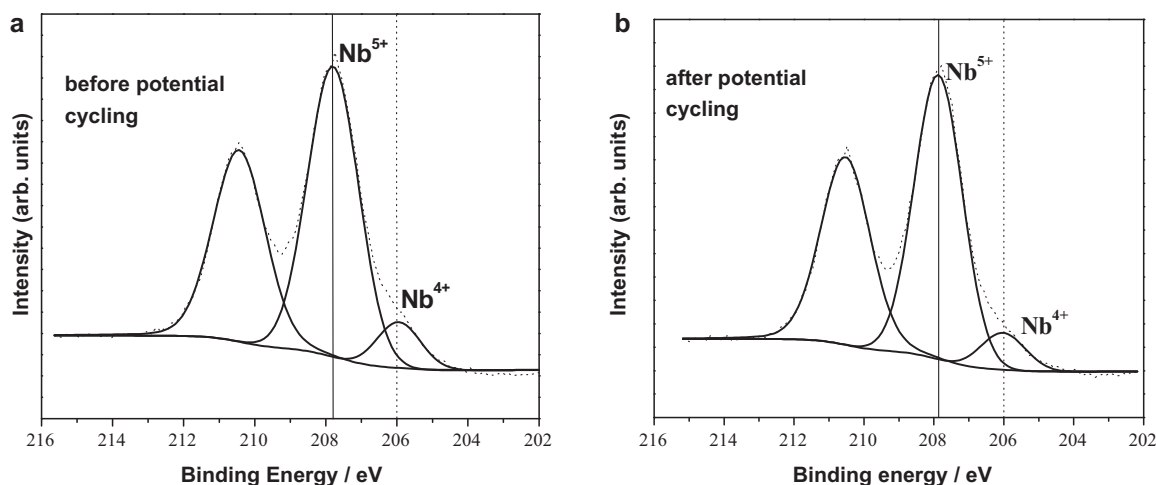


Fig. 9. High-resolution XPS spectra in the Nb^{3d} region of NbO₂ samples (a) before and (b) after electrochemical stability test up to 2000 cycles in N₂-saturated 0.1 M HClO₄ solution. The dashed and straight curves represent the original XPS curves and deconvoluted curves, respectively.

ORR mass activity of Pt/NbO₂ catalyst. The XPS spectrum of NbO₂ acquired after potential cycling (Fig. 9 (b)) is very much similar to the initial XPS spectrum Fig. 9 (a)). However, the ratio of Nb⁵⁺/Nb⁴⁺, calculated using the corresponding XPS peaks, is increased from 5.9 to 7.8 after the durability test, indicating that the electrochemical potential cycling could result in more insulating Nb₂O₅ on the NbO₂ nanofiber surface. Due to more insulating Nb₂O₅ is formed on the catalyst with increasing CV cycling, the drop in ORR mass activity should be understandable. This result approximately agrees with those observed and explained by Zhang et al. [20]. Similarly, Ti₄O₇ surface may also undergo a surface oxidation due to potential cycling. For example, Li et al. [21] reported the surface transformation of Ti₄O₇ into TiO₂, analyzed by XPS after the Ti₄O₇ was kept at 0.55 V vs. Hg/HgO for 360 h. We speculate that even though the Nb₂O₅ or TiO₂ layers, formed due to durability tests, may be fairly thin, their effect on electrical conductivity would be significant, which could create a poor electrical communication between the Pt catalyst particle with the nanofiber support, leading to a lower mass activity. Therefore, the rapid deterioration of mass activity may be attributed to two factors: (1) Nb₂O₅ or TiO₂ existence on the nanofiber surface limiting the electron transport between the Pt particle and the NbO₂ or Ti₄O₇ support; and (2) possible dissolution and agglomeration of Pt catalyst particles reducing the ORR reaction active surface area, which is evident by the decrease in ECSA (Fig. 7).

4. Conclusions

Two electronically conductive NbO₂ and Ti₄O₇ nanofibers were synthesized using a modified electrospinning technique in an effort to synthesize metal oxides as a possible replacement for carbon as PEM fuel cell catalyst support. The first step in the synthesis was to fabricate Nb and Ti metal oxide nanofibers, which then were transformed into NbO₂ and Ti₄O₇ nanofibers by a high temperature reduction treatment in H₂/N₂ environment. The synthesized nanofibers were physically characterized using several instrument methods such as XRD, EDX, SEM, TEM, BET as well as XPS. The thermal, chemical, and electrochemical stabilities as well as the electronic conductivities of these two supports were also evaluated in order to check their feasibility as catalyst supports in a temperature range 95–200 °C. Thermogravimetric analysis confirmed that NbO₂ is more prone to oxidation into a higher metal oxidation state (Nb₂O₅) at relatively lower temperatures (~150 °C) whereas the thermal stability of Ti₄O₇ is

relatively higher (~400 °C). Both supports are chemically stable in mild acidic conditions (1 M H₂SO₄) in the temperature range of 95–200 °C.

Pt catalysts, 20-wt% Pt/NbO₂ and 20-wt% Pt/Ti₄O₇, were also synthesized and tested for both ORR mass activity and stability in acidic solution. ORR mass activities obtained were 3.0 mA/mg Pt and 11.1 mA/mg Pt for 20-wt% Pt/NbO₂ and 20-wt% Pt/Ti₄O₇ catalysts, respectively, before the durability tests. After durability tests, these values dropped to 1.3 mA/mg Pt and 1.6 mA/mg Pt, indicating the ORR mass losses of 57% and 86% for 20-wt% Pt/NbO₂ and 20-wt% Pt/Ti₄O₇ catalysts, respectively. Through XPS measurements of the catalyst samples obtained before and after the durability tests, the formation of electronically insulating surface Nb₂O₅ on NbO₂ nanofibers was found to be responsible for low ORR mass activity and the catalyst degradation as well. Similar conclusions can be made for Ti₄O₇ based on literature findings that the formation of TiO₂ layer on Ti₄O₇, which adversely affects the electrochemical performance.

Acknowledgements

This work is part of Canadian National Technological Development Program (TDP), financially funded by National Research Council of Canada (NRC), Automotive Fuel Cell Cooperation (AFCC) Corp., Ballard Power Systems, and led by Ms. Maja Veljkovic. The authors would like to express their gratitude to Mr. Alan Guest, Dr. Dave Ghosh, Dr. Rod McMillan, Dr. Barry MacDougall, Dr. Christina Bock, Mr. Ryan Baker, Dr. Vladimir Neburchilov, and Dr. Chaojie Song from NRC, Ms. Shanna Knights from Ballard, and Dr. Harmeet Chhina from AFCC. Dr. Mark MacLachlan from the Department of Chemistry at the University of British Columbia is also highly appreciated for providing access to the thermogravimetric analyzer.

References

- [1] S.G. Chalk, J.F. Miller, *J. Power Sources* 159 (2006) 73.
- [2] K.-W. Park, K.-S. Seol, *Electrochem. Commun.* 9 (2007) 2256.
- [3] K. Sasaki, L. Zhang, R.R. Adzic, *Phys. Chem. Chem. Phys.* 10 (2008) 159.
- [4] K. Sasaki, R.R. Adzic, *J. Electrochem. Soc.* 155 (2008) B180.
- [5] T. Ioroi, Z. Siroma, N. Fujiwara, S. Yamazaki, K. Yasuda, *Electrochem. Commun.* 7 (2005) 183.
- [6] E.E. Farndon, D. Pletcher, *Electrochim. Acta* 42 (1997) 1281.
- [7] L. He, F. Franzen, D.C. Johnson, *J. Appl. Electrochem.* 26 (1996) 785.
- [8] J.R. Smith, F.C. Walsh, R.L. Clarke, *J. Appl. Electrochem.* 28 (1998) 1021.
- [9] G. Chen, S.R. Bare, T.E. Mallouk, *J. Electrochem. Soc.* 149 (2002) 1092.
- [10] D. Li, *Nano Lett.* 3 (2003) 555.

- [11] G. Larsen, R. Velarde-Oritz, K. Minchow, A. Barrero, I.G. Loscertales, *J. Am. Chem. Soc.* 125 (2003) 1154.
- [12] W. Wang, Z. Li, H. Huang, C. Wang, J. Sun, *Sens. Actuators B* 143 (2010) 745.
- [13] Y.Q. Chen, X.J. Zheng, X. Feng, *Nanotechnology* 21 (2010) 055708.
- [14] C.W. Jia, J.G. Zhao, H.G. Duan, E. Xie, *Mater. Lett.* 61 (2001) 4389.
- [15] D. Morris, Y. Dou, J. Rebane, C.E.J. Mitchell, R.G. Egdell, D.S.L. Law, A. Vittadini, M. Casarin, *Phys. Rev. B* 61 (2000) 13445.
- [16] J.M. Gallego, C.B. Thomas, *Thin Solid Films* 98 (1982) 11.
- [17] Y. Ou, X. Cui, X. Zhang, Z. Jiang, *J. Power Sources* 195 (2010) 1365.
- [18] M.D. Obradovic, B.M. Babic, A. Kowal, V.V. Panic, S.L. Gojkovic, *J. Serb. Chem. Soc.* 73 (2008) 1197.
- [19] S.-Y. Huang, P. Ganesan, B.N. Popov, *Appl. Catal. B: Environ.* 96 (2010) 224.
- [20] L. Zhang, L. Wang, C.M.B. Holt, T. Navessin, K. Malek, M. Eikerling, D. Mitlin, *J. Phys. Chem.* 114 (2010) 16463.
- [21] X. Li, A.L. Zhu, W. Qu, H. Wang, R. Hui, L.Z.J. Zhang, *Electrochim. Acta* 55 (2010) 5891.